PCCP

Accepted Manuscript

ROYAL SOCIETY OF CHEMISTRY

www.rsc.org/pccp

Table 1 Space group, lattice constant (Å), bond angle (°), mesh size (Å) of the two allotropes.

Systems	Space group	lattice constant	bond angle	mash size
C_y	Pmmm	a=9.428, c=17.388	∠1=122.923, ∠2=128.859,∠3=141.350	S1=3.591, S2=5.991, S3=5.200
C_Z	Pmmm	a=9.380, c=19.102	∠1=142.684, ∠2=132.224	S1=3.591, S2=4.517

force on each atoms converges to be less than 0.01 eV/Å.

To measure the thermodynamic stability of C_y and C_z, the molecular dynamics (MD) code LAMMPS[28] was carried out. The adaptive intermolecular reactive bond order (AIREBO) potential[29] was used to describe the C-C interaction with the cutoff distance of 3 Å. Periodic boundary conditions were used in the XZ plane. The simulations were performed in the NVT ensemble with the temperature controlled by the velocity scaling method. The time step of the simulations was set as 0.2 fs. The atoms used in the simulations were 11088 and 6144 for C_y and C_z, respectively. Meanwhile, the ab initio molecular dynamics (AIMD) simulation as implemented in CP2K/QUICKSTEP program package (http://www.cp2k.org)[30] was also performed to further confirm their thermodynamics stabilities. The CP2K package employs a mixed Gaussian and plane-wave basis set and norm-conserving pseudopotentials. The Kohn-Sham orbitals were expanded in the basis of Gaussian functions by employing double zeta valence polarized basis sets which are optimized for the GTH pseudopotentials (DZVP-MOLOPT-SR-GTH)[31]. A 400 Ry cut-off energy was used for plane-wave basis set. In the AIMD simulations the NVT ensemble was also used with a target temperature of 500 K, maintained with a Nosé-Hoover chain thermostat.

3 Results and Discussions

From the point of view of structure, using stable segment of existent carbon allotrope such as H-diamond, mutated H-diamond, and C-diamond we successfully proposed H-carbon and S-carbon in our previous work[32]. We call such method as segment combination method. With the main point of segment combination method, the 2D carbon allotropes can be constructed by choosing stable carbon based molecules as stable segment. In present work, we choose the molecular segment which has been synthesized in experiments[33] by which the new allotropes proposed in present work are hoping to be realized in experiments. Up to now, the monomer of hexaethynylbenzene[34], biphenylene[35] and carbyne[36] can be not only synthesized in experiments but also easily modulated. Using the three molecular segments as the basis, through first-principles relaxation we find two stable 2D carbon allotropes named as C_y and C_z composed purely of carbon atoms as

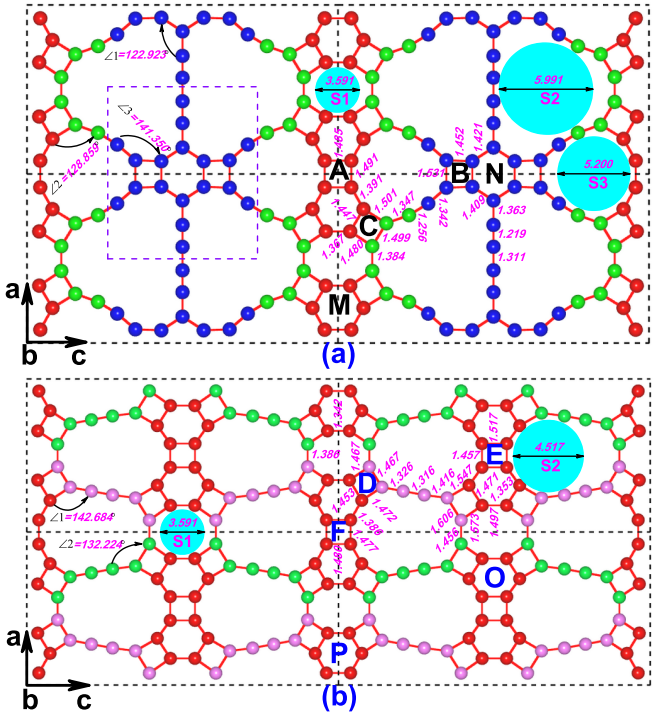

Fig. 1 (a) and (b) stand for the DFT-optimized structures of C_y and C_z, respectively. All spheres stand for carbon atoms. The green and pink sphere groups stand for carbyne chain; the blue and red sphere groups respectively stand for the monomer of dehydro-hexaethynylbenzene and biphenylene, respectively. The non-equivalence bonds and several important bond angles are labeled. The group lies in the violet rectangular dotted box stands for a monomer of dehydro-hexaethynylbenzene. The units of bond length and angles is "Å" and degree "°", respectively.

shown in Fig. 1 (a) and (b), respectively. Similar to the synthesized graphdiyne that can be constructed by dehydro-hexaethynylbenzene, C_y can be taken as organic combination of the three kinds of monomers mentioned above, as shown in Fig. 1 (a), where the blue, red, and green spheres respectively belong to dehydro-hexaethynylbenzene, biphenylene, and carbyne molecules, respectively. As for C_z, it can be built by only assembling biphenylene and carbyne molecules, as shown in Fig. 1 (b), where the green and pink spheres are part of carbyne chain and the red spheres belong to biphenylene molecule. Both C_y and C_z share the same space group Pmmm. They contain C4 squares, C6 hexagons, C8 octagons as well as 12, 14 and 18 rings. In the two structures, the bond length in different size polygon is unequal, such as C4 or C6 rings. Moreover, the bond lengths of two polygons with the same size are also different. For example, as shown in Fig 1. (a), C_y contains three kinds of C4 rings which are labeled as A, B and C, respectively. The value of the nonequivalent bond length of A ring is 1.485 and 1.491 Å whereas the nonequivalent bond length of B ring is 1.531 and 1.452 Å, and for C ring, the value is 1.447, 1.480, 1.499 and 1.501 Å. There are two types of C6 rings for C_y labeled as M and N, respectively. The similar situation can be also found for C_z, as shown in Fig. 1 (b). Meanwhile, C_y and C_z contain much short bond lengths ranging from 1.219 to 1.416 Å. Apparently, there are two kinds of hybridized carbon atoms in the two geometries, which is similar to graphyne family consisted of sp^2 and sp carbon atoms. Several important bond angles are also labeled in Fig. 1, where the angle value of 122.923° suggests sp^2 hybridization carbon atoms. The lattice constants of C_y and C_z are shown in Tab. 1. The results show that along $\vec{a}$ the lattice constant is nearly the same for the two structures, while along another periodic direction $\vec{c}$, the lattice constant of C_z is much larger than that of C_y.

As for the structure of the two systems, one interesting point is the specific well-defined mesh structures, as shown in Fig. 1. C_y contains three kinds of mesh labeled S1 (C8), S2 (C18) and S3 (C12). The diameter of them is 3.591, 5.991 and 5.200 Å. For C_z, two sized large meshes can be found, and the diameter of them is S1 (C8, its diameter is 3.591 Å) and S2 (C14, its diameter is 4.517 Å). This distinctive structure is similar to porous graphene[39,40], which is suitable for 2D molecular sieve.

To evaluate the stability of C_y and C_z, the formation energy with respect to graphene defined as E_f = [$E_{tot(sheet)}$ - NE_c]/N (where $E_{tot(sheet)}$ and E_c is the total energy of a corresponding unit cell of each carbon allotrope and an isolated carbon atom, respectively; N is the total number of carbon atoms in each unit cell) was calculated and the results are shown in Fig. 2. The relative formation energy of other four carbon allotropes including graphyne, graphdiyne, graphenylene, and carbyne are also included in the figure for com-

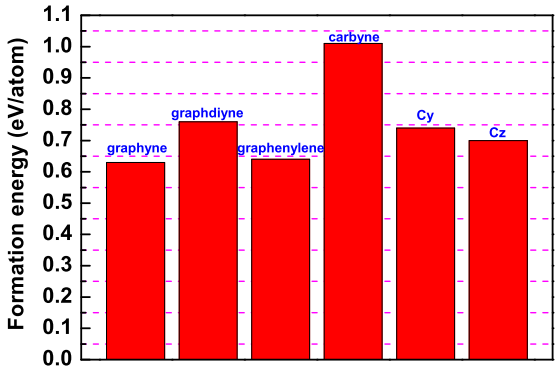

Fig. 2 Formation energy per atom of C_y and C_z as well as several other carbon allotropes for comparison purpose.

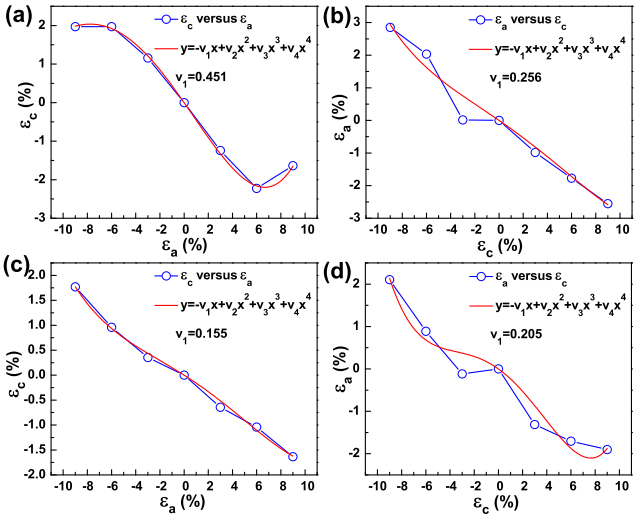

Fig. 3 (a) and (b) respectively stands for the ε_c versus ε_a and ε_a versus ε_c for C_y. (c) and (d) respectively stands for the ε_c versus ε_a and ε_a versus ε_c for C_z. The blue circles are calculated data which is fitted by function of y=-v_1x+v_2x^2+v_3x^3+v_4x^4 denoted by red line, with v_1 as the linear Poisson's ratio.

parison purpose. The results indicate that the stability sequence is graphene > graphenylene > graphyne > C_z > C_y > graphdiyne > carbyne. Although graphdiyne is much less favorable as compared to C_z and C_y due to its higher formation energy, it was synthesized in experiment [12] suggesting the great possibility for the synthesis of C_y and C_z. We further check their thermodynamic stabilities because only relatively lower energies are inadequate to determine the possible existence of C_y and C_z. Hence, AIMD simulation was performed under the temperature of 500 K, 1 fs time step, and NVT ensemble. $2\times1\times2$ supercells (which contains 168 and 192 carbon atoms for C_y and C_z, respectively) were adopted in AIMD simulations. We find that C_z and C_y maintain their initial configurations for 6 ps, which confirms their thermodynamical stabilities. The temperature in function of time steps in the AIMD simulations is shown in Fig. 3 (a) and (b) for C_y and C_z, respectively. The temperature stably fluctuates around 500 K. The potential energy of C_y and C_z in function of time steps in the simulation is also displayed in Fig. 1 (c) and (d), respectively. The results indicate that the potential energies of the two systems fluctuate around average value during the whole simulation time. Both above results confirm the possibility of their existence in reality under the temperature. Although the AIMD simulations can give credible results, it is difficult to simulate the thermodynamic stability of a system with a large scale atoms due to its restriction on the computational capabilities and time-consuming. Therefore, we in turn perform LAMMPS code to further verify thermodynamic stabilities of C_y and C_z. The simulations were carried out in the NVT ensemble with a time step of 0.2 fs at 1000 K and 1500 K for C_y and C_z, respectively. In the simulations, 11088 and 6144 atoms were used for C_y and C_z, respectively. The results indicate that the two geometries are preserved very well even after running 300 ps. Our recent work [38] reported that graphdiyne starts to produce defects when the temperature close to about 1200 K. The above results indicate that the stability of C_y are almost identical with graphdiyne, whereas C_z is more stable than graphdiyne.

The Poisson's ratio is an important physical parameter on account of the mechanical property of a material. In the following, we calculate the Poisson's ratios of C_y and C_z. When deformation is applied along $\vec{a}$ direction, the induced strain in the $\vec{c}$ direction and visa versa is shown in Fig. 3. As is shown in Fig. 3 (a), the calculated data (blue circular) behaves as a strongly nonlinear feature, which can be well fitted by function of $y=-v_1x+v_2x^2+v_3x^3+v_4x^4$. The linear parameter v_1 is fitted to be 0.451 and can be viewed as the linear Poisson's ratio in the $\vec{c}$ orientation. Similarly, the Poisson's ratio in the $\vec{a}$ orientation is 0.256, as shown in Fig. 3 (b). Obviously, as for C_y, the stiffiness in the $\vec{a}$ orientation is harder than that in $\vec{c}$ direction. For C_z, however, the stiffiness in the $\vec{a}$ orientation is softer than that in $\vec{c}$ direction. These results indicate that the

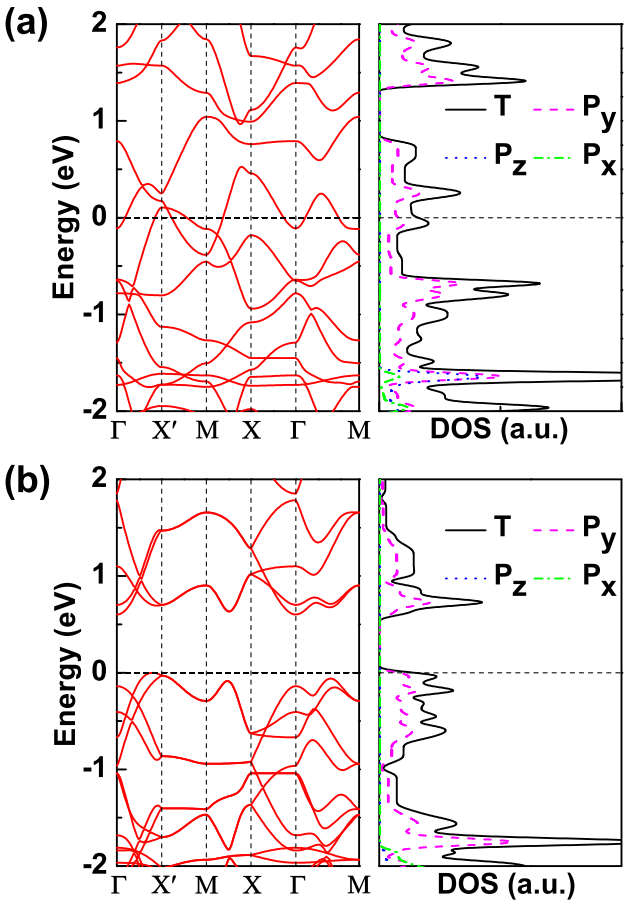

Fig. 4 Band structure and corresponding PDOS of C_y (a) and C_z (b), where the letter T stands for the total density of states of corresponding structures.

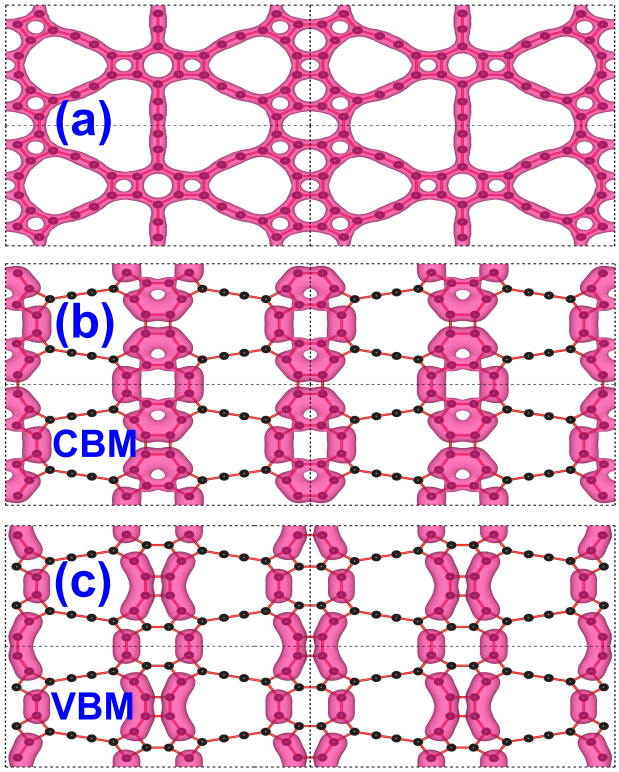

Fig. 5 (a) Charge density in a 2×2 unit cell of C_y. (b) and (c) respectively are the charge density of CBM and VBM of C_z. The isosurface of charge density is 0.0007 electron/Å^3.

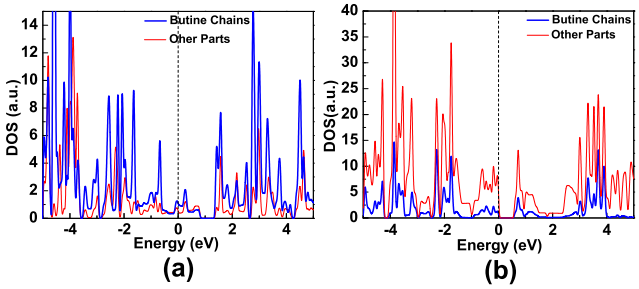

Fig. 6 Density of states (DOS) contributed by butine chains and other parts in the unit cell of (a)C_y and (b)C_z.

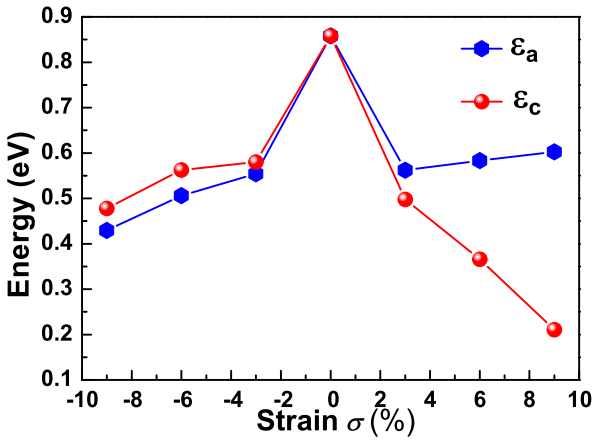

Fig. 7 Band gap of C_z in functions of strain.

mechanical properties of C_y and C_z are anisotropic.

We then further study the electronic properties of C_y and C_z based on the stable configuration obtained above. The calculated band structures and partial density of states (PDOS) of C_y and C_z are shown in Fig. 4 (a) and (b), respectively. The results indicate that the valence band of C_y pass through the Fermi level (E_f) indicating its metallic nature. The uniform charge density distribution of C_y as shown in Fig. 5 (a) indicates that C_y is a good conductor. As is shown in Fig. 6 (a), the states from the butine chains and other parts nearly have the same contribution to the states around the E_f, which results in the continuous distribution at butane chains and other parts. Naturally, the conductive feature of C_y is almost the same whether along $\vec{a}$ or $\vec{c}$ direction. The PDOS of C_y as shown in Fig. 4 (a) shows that the conduction electrons mainly come from the p_y (here y is the direction perpendicular to carbon layer) states of carbon atoms similar to the conductive origin of graphene. The band structures of C_z indicate that it behaves as an indirect semiconductor. Its conduction band minimum (CBM) locates at Γ point, whereas its valence band maximum (VBM) locates at the point between the Γ and X' point. The energy gap between VBM and CBM is 0.858 eV. The partial charge density of CBM and VBM is shown in Fig. 5 (b) and (c), respectively. In contrast to the case of C_y, as for C_z, the distribution of charge density is zero on the four carbon chains in the unit cell of C_z, which naturally splits the whole carbon sheet into independent one dimensional channels along x-axis. The DOS of CBM and VBM for C_z are mainly contributed by carbons other than butine chains, as shown in Fig. 6 (b), which is the essential reason of forming such stripe-like charge distribution. The strong continuous

localization of charge density along x-axis will give rise to anisotropic electronic conductivity in C_z structure. The distance between such stripe-like electron transport channels is up to 4.01 Å, by which a perfect 1D aligned electron transport is able to be realized in C_z structure. The anisotropic property of electronic transport in C_z structure may bring about potential applications in nano-electronics because 1D electronic channels can be applied as conducting wires in thin film transistor.

Considering the preparation and application of C_y and C_z should be supported on certain substrate, the lattice mismatch between the two structures and substrate is inevitable. The study of the dependence of the electronic structures of the two systems on strain effect is significant. We use uniaxial strain along axis $\vec{a}$ or axis $\vec{c}$ and the strain ranges from -9% (negative is compressed strain) to 9% (positive is tensile strain). As for C_y, within the strain range the system always keeps original metallic nature until a tensile strain along axis $\vec{a}$ approaches to 9% turning it into an indirect semiconductor. Within the strain scope (-9%, 9%), the type of the band gap of C_z maintains its unstrained indirect gap feature. However, the results as shown in Fig. 7 indicate that the energy gap of C_z is sensitively dependent on the in-plane uniaxial strain. When the strain is along $\vec{c}$ vector the band gap of C_z decreases with the increase in both stretch and compressed strain. The band gap can be tuned from 0.211 ($\sigma = 9\%$) to 0.858 eV ($\sigma = 0$). When the compression strain is along $\vec{a}$, the decrease trend of band gap is nearly identical to that along the $\vec{c}$ vector. The band gap decrease from 0.858 eV to 0.455 eV ($\sigma = -9\%$). However, under stretching strain along $\vec{a}$, the band gap decreases when the stretching strain is smaller than 3%, and then the band gap slightly increases when the strain is larger than 3%. To understand the reason that the band gap of C_z varies with the in-plane uniaxial strain, a detailed analysis was made as follows: under zero strain, the CBM of C_z locates at Γ point while its VBM locates between the Γ and X' points. When applying compression strain of -3% along $\vec{a}$ axis, we can find that from the Fig. S2 (a), the location of CBM shifts to the point between the X and Γ points, whereas VBM keeps unchanged. The energy of the CBM and VBM all decrease relative to Fermi level, but the decreasing amplitude of the CBM is larger than that of VBM. With increasing of compression strain, the location of CBM and VBM are nearly unchanged (the location of VBM under compression strain of -6% lies between M and X points), but the energy of CBM consistently decreases, whereas VBM continuously increases, which leads to the continuous decrease of the energy gap of C_z. The same conclusion can be found when applying compression strain along $\vec{c}$ axis, as shown in Fig. S2 (b). When applying tensile strain of 3% along $\vec{a}$ axis, the location of CBM jumps to the point between Γ and M points, whereas VBM nearly unchanged. In the process, the energy of CBM has a significant decrease in spite of the energy of VBM only shows a little decrease, which results in the decrease of band gap of C_z. With increasing of tensile strain further along $\vec{a}$ axis, however, the energy of CBM tends to have a slight increase, whereas the VBM nearly unchanged, thereby, the energy gap of C_z in turn starts increasing slightly. When applying tensile strain along $\vec{c}$ axis, the CBM shifts to the point between X and Γ points, whereas VBM shifts to the point between M and X point. With increasing of tensile strain, the energy of CBM and VBM continuously decrease and increase, respectively, which leads to the decreasing of the band gap of C_z, as shown in Fig. S2 (b). The above results indicate that the band gap of C_z can be significant adjusted by the in-plane strain, which will make C_z find interesting applications in nanoelectronics.

4 Conclusion

By performing the first-principles calculations, two novel 2D carbon allotropes named C_y and C_z with Pmmm symmetry are predicted to be energetically and thermodynamically stable. The Poisson's ratios of C_y and C_z show their anisotropic mechanical properties. The electronic structure calculations indicate that C_y is a metal and C_z is a semiconductor with band gap of 0.858 eV. The electronic conductivity of C_z is anisotropic in the direction of the two unit cell axis, moreover its band gap sensitively depends on in-plane strain. Meanwhile, their well-defined mesh structures are promising for gas molecular separation and storage.

Acknowledgement

This work was financially supported by the National Natural Science Foundation of China (Grant Nos. 11574260 and 11274262) and the Natural Science Foundation of Hunan Province, China (Grand No. 14JJ2046).

References

1 R. E. Smalley, H. Kroto, J. Heath, *Nature*, 1985 **318** 162.
2 S. Iijima, *Nature*, 1991 **354** 56.
3 K. S. Novoselov, A. K. Geim, S. Morozov, D. Jiang, Y. Zhang, S. Dubonos, I. Grigorieva, A. Firsov, *Science*, 2004 **306** 666.
4 K. Novoselov, A. K. Geim, S. Morozov, D. Jiang, M. K. I. Grigorieva, S. Dubonos, A. Firsov, *Nature*, 2005 **438** 197.
5 Y. Zhang, Y.-W. Tan, H.L. Stormer, P. Kim, 2005 *Nature*, **438** 201.
6 A.K. Geim, K.S. Novoselov, *Nat. Mater.*, 2007 **6** 183.
7 X. Luo, L.-M. Liu, Z. Hu, W.-H. Wang, W.-X. Song, F. Li, S.-J. Zhao, H. Liu, H.-T. Wang, Y. Tian, *J. Phys. Chem. Lett.*, 2012 **3** 3373.
8 J. Chen, J. Xi, D. Wang, Z. Shuai, *J. Phys. Chem. Lett.*, 2013 **4** 1443.
9 C. Eda, M. Chhowalla, *Adv. Mater.*, 2010 **22** 2392.

10 H. Tang, C.M. Hessel, J. Wang, N. Yang, R. Yu, H. Zhao, D. Wang, *Chem. Soc. Rev.*, 2014 **43** 4281.
11 Y. Wang, Z. Li, J. Wang, J. Li, Y. Lin, *Trends in Biotechnology*, 2011 **29** 205.
12 R.H. Baughman, H. Eckhardt, M. Kertesz, *J. Chem. Phys.*, 1987 **87** 6687.
13 G. Li, Y. Li, H. Liu, Y. Guo, Y. Li, D. Zhu, *Chem. Commun.*, 2010 **46** 3256.
14 B.G., Kim, H.J., Choi, *Phys. Rev. B*, 2012 **86** 115435.
15 D. Malko, C. Neiss, F. Viñes, A. Görling, *Phys. Rev. Lett.*, 2012 **108** 086804.
16 C.-H. Park, L. Yang, Y.-W. Son, M.L. Cohen, S.G. Louie, *Nat. Phys.*, 2008 **4** 213.
17 C.-H. Park, Y.-W. Son, L. Yang, M.L. Cohen, S.G. Louie, *Nano Lett.*, 2008 **8** 2920.
18 W.-J. Yin, Y.-E. Xie, L.-M. Liu, R.-Z. Wang, X.-L. Wei, L. Lau, J.-X. Zhong, Y.-P. Chen, *J. Mater. Chem. A*, 2013 **1** 5341.
19 Q. Song, B. Wang, K. Deng, X. Feng, M. Wagner, J.D. Gale, K. Mllen, L. Zhi, *J. Mater. Chem. C*, 2013 **1** 38.
20 G. Brunetto, P.A.S. Autreto, L.D. Machado, B.I. Santos, R.P.B. dos Santos, D.S. Galvão, *J. Phys. Chem. C*, 2012 **116** 12810.
21 X.Q. Wang, H.D. Li, J.T. Wang, *Phys. Chem. Chem. Phys.*, 2013 **15** 2024.
22 C. Su, H. Jiang, J. Feng, *Phys. Rev. B*, 2013 **87** 075453.
23 G. Kresse, J. Furthmüller, *Phys. Rev. B*, 1996 **54** 11169.
24 G. Kresse, J. Furthmüller, *Comput. Mater. Sci.*, 1996 **6** 15.
25 J.P. Perdew, K. Burke, M. Ernzerhof, K. Burke, *Phys. Rev. Lett.*, 1996 **77** 3865.
26 G. Kresse, D. Joubert, *Phys. Rev. B*, 1999 **59** 1758.
27 P.E. Blöchl, *Phys. Rev. B*, 1994 **50** 17953.
28 S. Plimpton, *Comput. Mater. Sci.*, 1995 **117** 1.
29 S.J. Stuart, A.B. Tutein, J.A. Harrison, *J. Chem. Phys.*, 2000 **112** 6472.
30 J. VandeVondele, M. Krack, F. Mohamed, M. Parrinello, T. Chassaing, J. Hutter, *Comput. Phys. Commun.*, 2005 **167** 103.
31 J. VandeVondele, J. Hutter, *J. Chem. Phys.*, 2007 **127** 114105.
32 C. He, L.Z. Sun, C. X. Zhang, X. Y. Peng, K. W. Zhang, and J. Zhong, *Sol. Stat. Comm.*, 2012 **152** 1560.
33 G.R. Desiraju, *J. Am. Chem. Soc.*, 2013 **135** 9952.
34 R. Diercks, J.C. Armstrong, R. Boese, K.P.C. Vollhardt, *Angew. Chem. Int. Ed.*, 1986 **25** 268.
35 W.C. Lothrop, *J. Am. Chem. Soc.*, 1941 **63** 1187.
36 W.A. Chalifoux, R.R. Tykwinski, *Nat. Chem.*, 2010 **2** 967.
37 M. Liu, V.I. Artyukhov, H. Lee, F. Xu, B.I. Yakobson, *ACS Nano*, 2013 **7** 10075.
38 S.Y. Ma, M. Zhang, L.Z. Sun, K.W. Zhang, *Submitted to Carbon*
39 Y. Li, Z. Zhou, P. Shen, Z. Chen, *Chem. Commun.*, 2010 **46** 3672.
40 D. Jiang, V.R. Cooper, S. Dai, *Nano Lett.*, 2009 **9** 4019.